Vol. 74: 263–281, 2018
https://doi.org/10.3354/cr01500

CLIMATE RESEARCH
Clim Res

Published online February 28

Nonlinear changes in aridity due to precipitation and evapotranspiration in China from 1961 to 2015

Yunhe Yin[1,*], Danyang Ma[1,2], Shaohong Wu[1,2]

[1]Key Laboratory of Land Surface Pattern and Simulation, Institute of Geographic Sciences and Natural Resources Research, Chinese Academy of Sciences, Beijing 100101, PR China

[2]University of Chinese Academy of Sciences, Beijing 100049, PR China

ABSTRACT: Changes in regional aridity have complicated spatio-temporal features during the past several decades and have important implications for hydrologic cycles under global climate change. However, nonlinear changes in aridity and its spatial variability in China remain poorly understood. Here, we analyzed the spatial-temporal changes in hydroclimatic variables, including reference evapotranspiration (ET_o), precipitation (P), aridity index (AI) and their relationships, mainly based on the ensemble empirical mode decomposition method. A climate dataset from 573 meteorological stations in China was used for the period 1961–2015. The results show that the nonlinearity of changes in aridity was complex, with distinct spatial differences. Approximately 76.09% of stations showed reversed trends in AI during 1961–2015, among which AI initially decreased and then increased, mainly in Inner Mongolia and the areas south of the middle and lower reaches of the Yangtze River. However, their reversal times were not synchronous. The drying to wetting transition mainly occurred in northern areas, including the southern part of Northeast China, the eastern Loess Plateau and the southern North China Plain. Although the majority of stations experienced reversals from downward to upward trends of ET_o (53.92%) mainly around the 1990s, increasing precipitation exerted a larger effect on AI. For most eco-geographical regions in China, the nonlinear variations in ET_o and P jointly led to the decline in AI over the past 55 yr, and the P trend contributed more than the ET_o trend to the change in AI, except in subtropical regions, where ET_o variations played a key role.

KEY WORDS: Aridity · Precipitation · Reference evapotranspiration · Nonlinear · Climate change · Ensemble empirical mode decomposition · EEMD

1. INTRODUCTION

Aridity or humidity are important hydroclimatic characteristics sensitive to climate change (McCabe & Wolock 2002) and greatly influence water resources management, ecosystem function, agricultural production and desertification control. Under climate change, there is a likelihood of changes in aridity with complicated spatial-temporal features and significant implications for hydrologic cycles. Drier or wetter conditions can be effectively identified by capturing the changes in the background aridity (Sherwood & Fu 2014, Roderick et al. 2015), which is an essential requirement to interpret landscape characteristics and to make reasonable use of water resources (Kukal & Irmak 2016). Variations in aridity have a remarkable impact on annual runoff rates (Arora 2002) and links to biogeochemical dynamics that influence key ecosystem functions and services (Delgado-Baquerizo et al. 2013). For example, if aridity increases in the future, trees are likely to suffer considerably reduced growth (Williams et al. 2010).

High spatial and temporal variability in aridity has occurred over the last few decades. Recently, ob-

*Corresponding author: yinyh@igsnrr.ac.cn

served trends in global dryness have exposed contradictions, and large uncertainties still exist (Sheffield et al. 2012, Dai 2013, Feng & Fu 2013, Greve et al. 2014, Trenberth et al. 2014, Mueller & Zhang 2016). Regionally, increases in aridity have been revealed in southwestern Spain during 1951–2010 (Moral et al. 2017) and Iran during 1966–2005 (Tabari & Aghajanloo 2013). In contrast, wetter trends have been reported in the eastern US, as indicated by statistically significant increases in precipitation (P) minus reference evapotranspiration (ET_o) during 1895–1990 (McCabe & Wolock 2002). Moreover, a downward trend in aridity has been found in Northwest China (Huo et al. 2013), and 91.7% of the wetter trend has been attributed to increasing precipitation from 1960–2010 (Liu et al. 2013).

Considering changes in the hydroclimatic system, it has been suggested that aridity is controlled by a joint effect of climatic supply of water (P) and the atmospheric evaporative demand (e.g. ET_o) (McCabe & Wolock 2002, Cook et al. 2014, Greve & Seneviratne 2015, Zarch et al. 2015, Huang et al. 2016). In particular, the latter plays a significant role in global atmosphere–hydrosphere–biosphere interactions (Wu et al. 2006). Overall, evidence from early observational and modeling studies has agreed on the decreasing trends of annual atmospheric evaporative demand at regional to continental scales during the past half-century (Peterson et al. 1995, Schimel et al. 1997, Roderick & Farquhar 2002, Hobbins et al. 2004, Dolman & de Jeu 2010, Wu et al. 2010, McVicar et al. 2012a, Kukal & Irmak 2016).

Indeed, recent studies stated that global and regional warming trends are nonlinear (Franzke 2014, Good et al. 2015). Similarly, nonlinear processes have been detected in precipitation (Xue et al. 2005, Chang et al. 2015) and aridity (Zhao et al. 2014, Li et al. 2015), with multi-scale changes over a relatively long period. The nonlinear changes in aridity during the past several decades have usually been diagnosed based on methods such as wavelet analysis and ensemble empirical mode decomposition (EEMD). These methods have also been applied to hydrologic factors such as runoff and groundwater, and have produced meaningful results (Partal 2012, Carmona & Poveda 2014, Yu & Lin 2015).

Particularly, EEMD, proposed by Wu & Huang (2009), is an effective time-series signal processing method, especially for nonlinear and nonstationary time series (Qian et al. 2009, Xue et al. 2013, Qian & Zhou 2014, Guo et al. 2016). For example, Li et al. (2015) and Sun & Ma (2015) used EEMD to analyze the temporal and spatial variations in the Palmer drought severity index and its influencing factors. Moreover, it was possible to extract representative scale exponents from precipitation data using EEMD to help construct regional intensity–duration–frequency curves (Kuo et al. 2013); it was also possible to predict the future long-term evolution of precipitation patterns using a stochastic model combining the EEMD method and non-parametric techniques (Basha et al. 2015). However, nonlinear changes in aridity remain poorly understood and need to be investigated — especially in countries with several different climates, such as China — in order to comprehensively understand regional climate change and its effects.

The major objectives of this study were (1) to explore the nonlinear variations in hydroclimatic variables including precipitation, reference evapotranspiration and aridity using the EEMD method during the period 1961–2015; (2) to analyze the spatial characteristics of nonlinear variations in aridity; and (3) to quantify their contributions to changes in aridity and its relationships with large-scale climatic oscillations. Investigating aridity variations provides a reliable way to detect and quantify the response of hydrological processes to climate change in detail, and provides useful information for agricultural water management.

2. MATERIALS AND METHODS

2.1. Materials

A total of 573 meteorological stations (Fig. 1) with high-quality monthly data for the period 1961–2015, which include minimum and maximum temperatures, wind speed, relative humidity and sunshine duration, were obtained from the Climatic Data Center (CDC) of the National Meteorological Information Center (NMIC) of the China Meteorological Administration (CMA). Missing data were estimated by averaging values from observations in other years for the same station.

In this study, the sea surface temperature anomaly (SSTA) over the Nino 3.4 region (5° N–5° S, 120–170° W) was selected as the indicator of El Niño/Southern Oscillation (ENSO) and downloaded from the Climate Prediction Center of the National Oceanic and Atmospheric Administration (NOAA). The monthly Nino 3.4 SSTA values during 1961–2015 were calculated based on centered 30 yr base periods updated every 5 yr, in order to remove the warming trend in the recent decades. The Pacific Decadal Oscillation (PDO) is often deemed as a long-lived

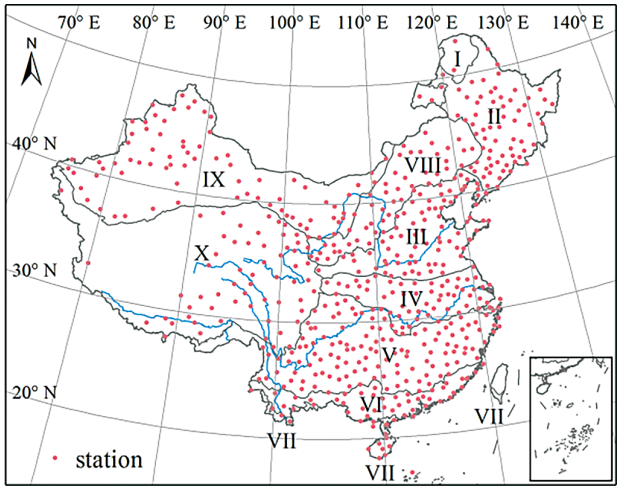

Fig. 1. Meteorological stations (red dots) used in this study and eco-geographical regions in China. I: Cold temperate humid region, II: mid-temperate humid/sub-humid region, III: warm temperate humid/sub-humid region; IV: north subtropical humid region; V: mid-subtropical humid region; VI: south subtropical humid region; VII: tropical humid region; VIII: north semi-arid region; IX: northwest arid region; X: Tibetan Plateau alpine region

El Niño-like pattern of Pacific climate variability (Zhang et al. 1997), and the monthly PDO index for 1961–2015 was obtained from NOAA's National Centers for Environmental Information.

China is characterized by a broad range of climate types, from tropical to cold-temperate and from humid to arid, with correspondingly diverse ecosystems. The distribution of eco-geographical regions adopted from Zheng (2000) (Fig. 1) was used in this study to describe the spatial differences of variation in aridity over China.

2.2. Aridity index

In this study, the aridity index (AI) is defined as the ratio of annual reference evapotranspiration (ET_o) over precipitation (P). It is widely used to reflect regional aridity or humidity conditions, and high values of the index indicate stronger aridity (Liu et al. 2013, Yin et al. 2015). It is a direct indicator of climatic moisture conditions. The contributions of annual ET_o and P to aridity change can be assessed in a straightforward way by using AI.

Modeling is a common approach to obtain ET_o. In 1998, the Food and Agricultural Organization (FAO) modified the Penman–Monteith model (hereafter FAO56-PM model) by defining a hypothetical reference crop closely resembling an extended surface of green grass of uniform height, vigorously growing, completely covering the ground and sufficiently watered. The model integrates mass transfer and energy balance and considers vegetation morphological characters, and it has proven to be valid in both arid and humid climates (Allen et al. 1998). The FAO56-PM model has been applied widely around the world. In this model, ET_o is calculated according to:

$$ET_o = \frac{0.408\Delta(R_n - G) + \gamma \frac{900}{T+273} U_2(e_s - e_a)}{\Delta + \gamma(1 + 0.34U_2)} \quad (1)$$

where R_n is the net radiation (MJ m^{-2}), G is the soil heat flux (MJ m^{-2}), γ is the psychrometric constant (kPa °C^{-1}), Δ is the slope of the saturation vapor pressure curve (kPa °C^{-1}), T is the average temperature (°C), U_2 is the wind speed at 2 m height (m s^{-1}), e_s is the mean saturation vapor pressure (kPa), and e_a is the actual vapor pressure (kPa).

Radiation in the model can be calculated through an empirical formula, and its accuracy is determined by empirical coefficients which have regional limitations. In this study, ET_o was calculated using the radiation-modified FAO56-PM model. The modified net radiation (Yin et al. 2008) was:

$$R_n = 0.77 \times \left(0.20 + 0.79\frac{n}{N}\right) R_{so} - \sigma \left[\frac{T_{x,k}^4 + T_{n,k}^4}{2}\right] \times (0.56 - 0.25\sqrt{e_a}) \left(0.1 + 0.9\frac{n}{N}\right) \quad (2)$$

where σ is the Stefan-Boltzmann constant (4.903 × 10^{-9} MJ K^{-4} m^{-2} d^{-1}), $T_{x,k}$ and $T_{n,k}$ are the maximum and minimum temperatures in Kelvin, respectively, n is actual sunshine hours, N is potential sunshine hours, and R_{so} is the clear-sky solar radiation.

2.3. EEMD method

The EEMD (Huang & Wu 2008, Wu & Huang 2009) is generally an adaptive time series analysis approach with the addition of noise. It works well in extracting long-term trends and oscillatory components characterized by multiple scales from complex signals, which makes it appropriate to address nonlinear and nonstationary processes. The EEMD inherits the advantages of its predecessor, empirical mode decomposition (EMD; Huang et al. 1998), in terms of processing signals and analyzing time-frequency characteristics. Meanwhile, the mode-mixing problem found in the EMD is resolved to guarantee the physical uniqueness of intrinsic mode functions (IMFs). Moreover, no *a priori* assumption is required

for the EEMD, which decomposes data on a basis of local features. Recently, EEMD has been gradually incorporated in the field of climatic change (Wu et al. 2011, Franzke 2012, Ji et al. 2014, Li et al. 2017), among which studies focusing on hydrological elements such as precipitation and evapotranspiration have mostly concentrated on the regional scale.

The key thought of the EEMD method is adding white noise to the original sequence $x(t)$ and decomposing the mixed data into a number of amplitude-frequency modulated oscillatory components C_j (j = 1, 2, …, m) and a residual component R_m as in Eq. (3):

$$x(t) = \sum_{j=1}^{m} C_j(t) + R_m(t) \quad (3)$$

where t corresponds to the time in years (t = 1961, 1962, 1963, …, 2015), C_j is a finite set of oscillatory functions known as IMFs, and R_m is a monotonic curve or contains at most 1 extreme.

The added white noise could cancel out with enough trials to achieve the adaptive decomposition within the dyadic filter windows. Finally, the IMFs will be acquired from the ensemble means through repetition of the above procedures. IMFs reflect the fluctuations of hydroclimatic variables with high frequency to low frequency, and vary unevenly with time. The number and attributes of IMFs rely exclusively on the data length and local features. The residue R_m is monotonic or includes no more than 1 extreme, which is assumed to have eliminated inherent fluctuations and retained secular trends indicating the true information of the signal. The trend varies with time, yet does not depend upon any given shape. It can reflect the potential, nonlinear and non-stationary characteristics of a time series more effectively than traditional linear fitting methods.

To obtain spatially-temporally coherent information, we first performed EEMD at each meteorological station with the same data length. Four IMFs and the final remainder were obtained from the 55 yr time series for each station over the whole area. The oscillatory components on similar timescales from all stations were then pieced together to form the spatial structural evolution of that timescale. Likewise, the secular trends were displayed by instantaneous rates, varying with time and space. The method could be deemed as a type of multi-dimensional EEMD, which combines the spatial and temporal locality, and is conducive to the diagnosis of climate system evolution (Ji et al. 2014).

In this study, the time series were augmented with white noise for 100 trials, when applying the EEMD to yearly data. The amplitude value was 0.2. A Monte Carlo method was implemented to test the statistical significance of the IMF, indicating whether it contained information with actual physical meaning at a given confidence level (Wu & Huang 2004). IMF components with mean periods of 1–10 yr and 10–50 yr are regarded as interannual and interdecadal variability, respectively. Considering the data length limitation, multidecadal variability in the case of a mean period of >50 yr was not studied.

The changing rate (Rate(t)) of the residual trend is determined by its temporal derivatives as in Eq. (4). To reflect the spatial pattern of nonlinear changes, we selected the changing rates of 5 years, i.e. 1970, 1980, 1990, 2000 and 2010:

$$\mathrm{Rate}(t) = \mathrm{d}R_m(t) / \mathrm{d}t \quad (4)$$

where $\mathrm{d}R_m(t)$ and $\mathrm{d}t$ indicate the differentials of $R_m(t)$ and t, respectively, and $\mathrm{d}R_m(t)/\mathrm{d}t$ is the first derivative of $R_m(t)$ versus t.

2.4. Linear trends and significance test

Linear regression analysis was used to detect linear trends in annual ET_o, P and AI from 1961–2015. The slope of the regression, calculated by ordinary least squares, was used to quantify linear trends (slope) over time as in Eq. (5):

$$\mathrm{slope} = \left[s\sum_{i=1}^{s} t \times x(t) - \sum_{i=1}^{s} t \sum_{i=1}^{s} x(t) \right] / \left[s\sum_{i=1}^{s} t^2 - \left(\sum_{i=1}^{s} t \right)^2 \right] \quad (5)$$

where i denotes the index of the year (i = 1, 2, 3, …, s), and s is the total number of years (s = 55). The positive slope indicates an increasing trend in the annual average variable during the period 1961–2015, and vice versa.

In addition, we used a non-parametric Mann–Kendall trend test (Sneyers 1990) to determine the statistical significance levels of the linear trends in annual hydroclimatic variables in 1961–2015.

2.5. Contribution assessment

To quantitatively investigate the contributions of ET_o and P to the AI, the trends of ET_o and P series, respectively, were removed to recalculate the AI. The difference between the original and recalculated AI could then be derived. The ratio of the difference divided by the original AI was perceived as the change in AI caused by the ET_o or P trend.

Note that when subtracting the residual trend from the original series, the trend value at the starting

time of 1961 was added to guarantee the comparability of the detrended and original data as in Eq. (6) below. The time series tended to be stationary after the trend was removed, with the first data value remaining unchanged. Using detrended ET_o and original P, or using original ET_o and detrended P, the AI was recalculated and compared with its original, generating the changing ratio of the difference in the AI as in Eqs. (7) and (8). It also varied with time due to the time-varying nature of the EEMD trend:

$$x_{\text{detrend}}(t) = x(t) - R_m(t) + R_m(1961) \quad (6)$$

$$\text{Ratio}_{ET_o}(t) = \frac{\text{AI}(t) - \frac{ET_{o\text{Detrend}}(t)}{P(t)}}{\text{AI}(t)} \times 100\% \quad (7)$$

$$\text{Ratio}_{P}(t) = \frac{\text{AI}(t) - \frac{ET_o(t)}{P_{\text{Detrend}}(t)}}{\text{AI}(t)} \times 100\% \quad (8)$$

3. RESULTS

3.1. Changes in reference evapotranspiration

EEMD was performed at each station to decompose the annual ET_o time series from 1961–2015, so that the spatial distribution of the mean periods for each IMF component could be obtained. Fig. 2 shows the spatial distributions of the mean period of the EEMD components of IMF1, IMF2, IMF3 and IMF4 for annual ET_o. It showed that IMF1 at most stations represented a quasi 3 yr oscillation but was not statistically significant. The IMF2 components were mainly 5 and 6 yr quasi-periodic oscillations, with significant periods primarily distributed in Northwest China and the Tibetan Plateau. Mean periods of IMF3 were predominantly 11 yr in the southeast and 14 yr in the northwest, approximately 31% of which

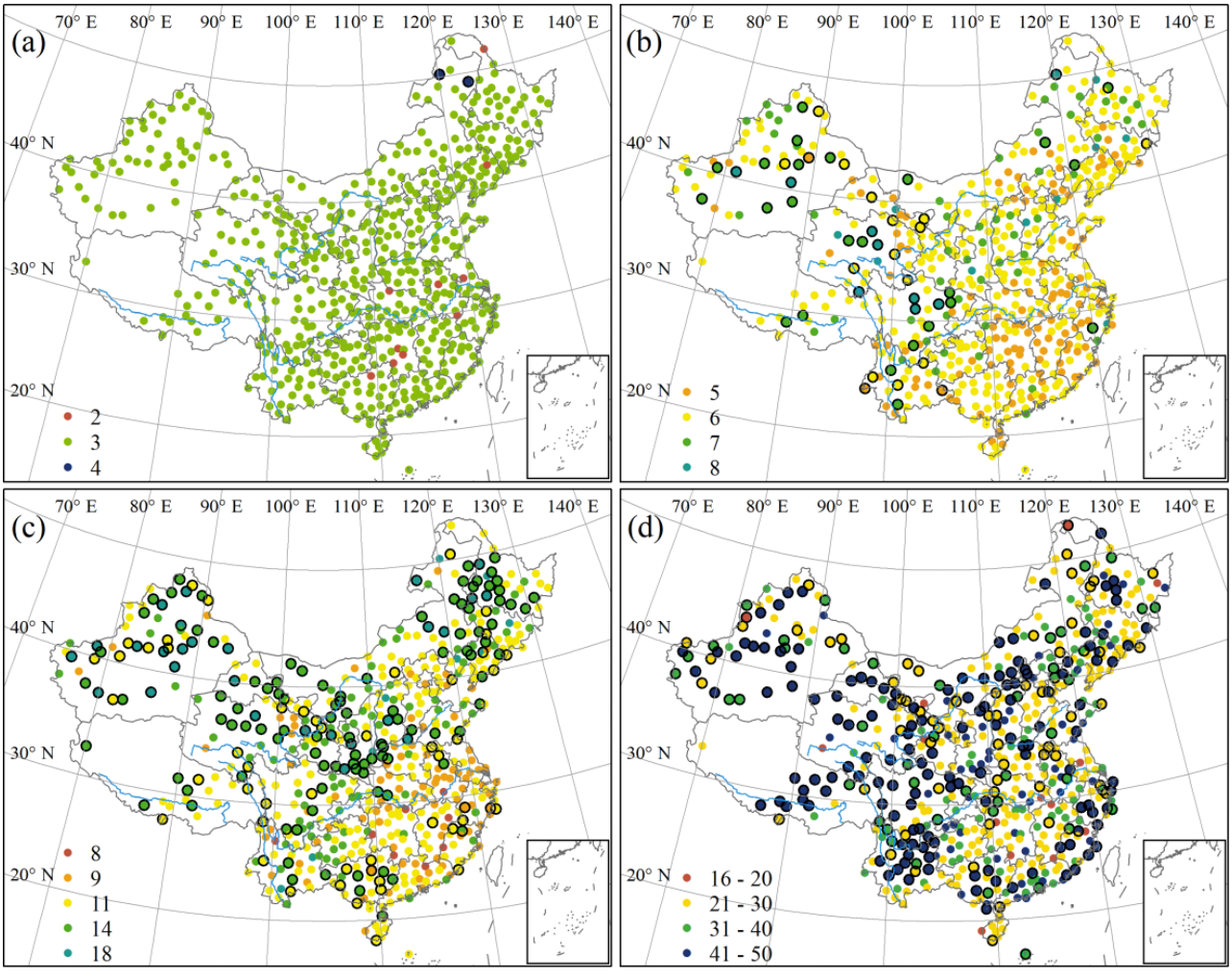

Fig. 2. Mean period of the ensemble empirical mode decomposition (EEMD) components (a) intrinsic mode function 1 (IMF1), (b) IMF2, (c) IMF3 and (d) IMF4 for annual reference evapotranspiration (unit: year). Note that circles with an outline indicate statistical significance ($p < 0.05$)

were statistically significant, concentrated in the Northeast Plain, Northwest China and the Tibetan Plateau. IMF4, at more than 42% of stations, showed obvious oscillations, with main periods of 21–30 yr in the southeast and 41–50 yr in the northwest. The spatial pattern of the IMF mean periods indicated that annual ET_o had longer period variations in the northwest than the southeast.

By calculating the temporal derivatives of the residual series based on EEMD, the changing rate of annual ET_o at each station could be obtained. Fig. 3a–e shows the spatial distributions of changing rates in 1970, 1980, 1990, 2000 and 2010, respectively. The most striking nonlinear changes occurred in the areas south of the middle and lower reaches of the Yangtze River, where annual ET_o were mainly decreasing by >2 mm yr^{-1} in 1970, but weakened in 1980 and translated into increases for some stations in 1990, with changing rates of −2~2 mm yr^{-1}. Most annual ET_o in this area exhibited increasing trends in 2000 with more considerable rates, reaching over 2 mm yr^{-1} in 2010 for most stations. Other areas where annual ET_o showed a decreasing to increasing trend included the eastern Inner Mongolian Plateau and parts of Northwest China, while the opposite changes were presented in places such as North China and the southern Tibetan Plateau.

Comparatively, the results show that annual ET_o at most stations (40.84%) displayed obvious negative linear trends in 1961–2015 across much of the country, based on the linear trend analysis. Only a small number of stations (11.17%), scattered across the study region, showed significant positive linear trends in ET_o (Fig. 3f).

Fig. 4 presents the EEMD components and linear trends of hydroclimatic variables averaged over the 573 stations during 1961–2015. Generally, IMF1 and IMF2 represent interannual variability, and IMF3 and IMF4 represent interdecadal variability. ET_o had quasi 3 yr and quasi 6 yr interannual scale oscillations, as well as quasi 11 yr and quasi 35 yr interdecadal scale oscillations (Fig. 4a). IMF4 was statistically significant at the 99% confidence level. ET_o anomalies relative to the average of 1961–2015 were mainly positive in the 1960s and 1970s, were negative from the 1980s to the early 2000s, and returned to positive in the mid- to late 2000s (Fig. 4b). The linear trend in annual ET_o was −0.65 ± 1.64 mm yr^{-1} ($p < 0.01$) for the period 1961–2015. There was also an obvious nonlinear change, indicated by the EEMD residual trend of annual ET_o, which was generally divided into 2 stages by 1997, decreasing to increasing, with averages rate of −1.19 and 0.58 mm yr^{-1}, respectively.

3.2. Changes in precipitation

Fig. 5 shows the spatial distributions of the period of EEMD components IMF1, IMF2, IMF3 and IMF4 for annual *P*. During 1961–2015, the main periods of the IMF1, IMF2 and IMF3 components of annual *P* were similar with those of annual ET_o. However, there were only a few stations that had significant periods. Specifically, IMF2 with significant mean periods only occurred in about 5% of the stations, which were mainly located in Southwest China and western Northwest China. Stations that had significant interdecadal periods of IMF3 and IMF4 were scattered across Northwest and South China. In addition, mean periods of IMF4 ranged between 21 and 30 yr, especially in the northwest, where the periods were much shorter than those for annual ET_o.

Over the past 55 yr, the patterns of changes in annual *P* have been spatially heterogeneous (Fig. 6). From the respective EEMD trends, the spatial patterns of changing rates in 1970, 1980 and 1990 were similar, i.e. increases in Southeast China, Northwest China and the Tibetan Plateau, with the exception of an area of decreasing *P* in 1990 that was enlarged to western Northeast China. However, areas with positive rates gradually expanded from 2000, especially for southern Northeast China and North China, where annual *P* began to increase. During the same period, areas with negative rates shrank, such as the areas south of the middle and lower reaches of the Yangtze River and eastern Inner Mongolia, where annual *P* first increased and then decreased. By 2010, approximately 61% of the stations showed an increasing trend, among which annual *P* in the eastern areas generally increased faster than 2 mm yr^{-1}. From the perspective of a linear trend, annual *P* had statistically significant increasing trends (10.47%) on the southeast coast, northwest inland and the Tibetan Plateau and significant decreasing trends (2.62%) in the Loess Plateau and southwestern areas over the study period (Fig. 6f). Comparatively, the linear trends mainly reflected the patterns of variability in annual *P* before 1990, but as for the inconsistent changes after 1990, variability in annual *P* could only be unraveled through the nonlinear analysis.

With reference to the station-averaged data, annual *P* had the same interannual variation periods with ET_o, but with interdecadal variation periods of quasi 14 yr and quasi 24 yr (Fig. 4c). Fig. 4d shows that the annual *P* anomalies oscillated around zero during the study period, with an insignificant linear trend of 0.18 ± 1.93 mm yr^{-1}. More specifically, the

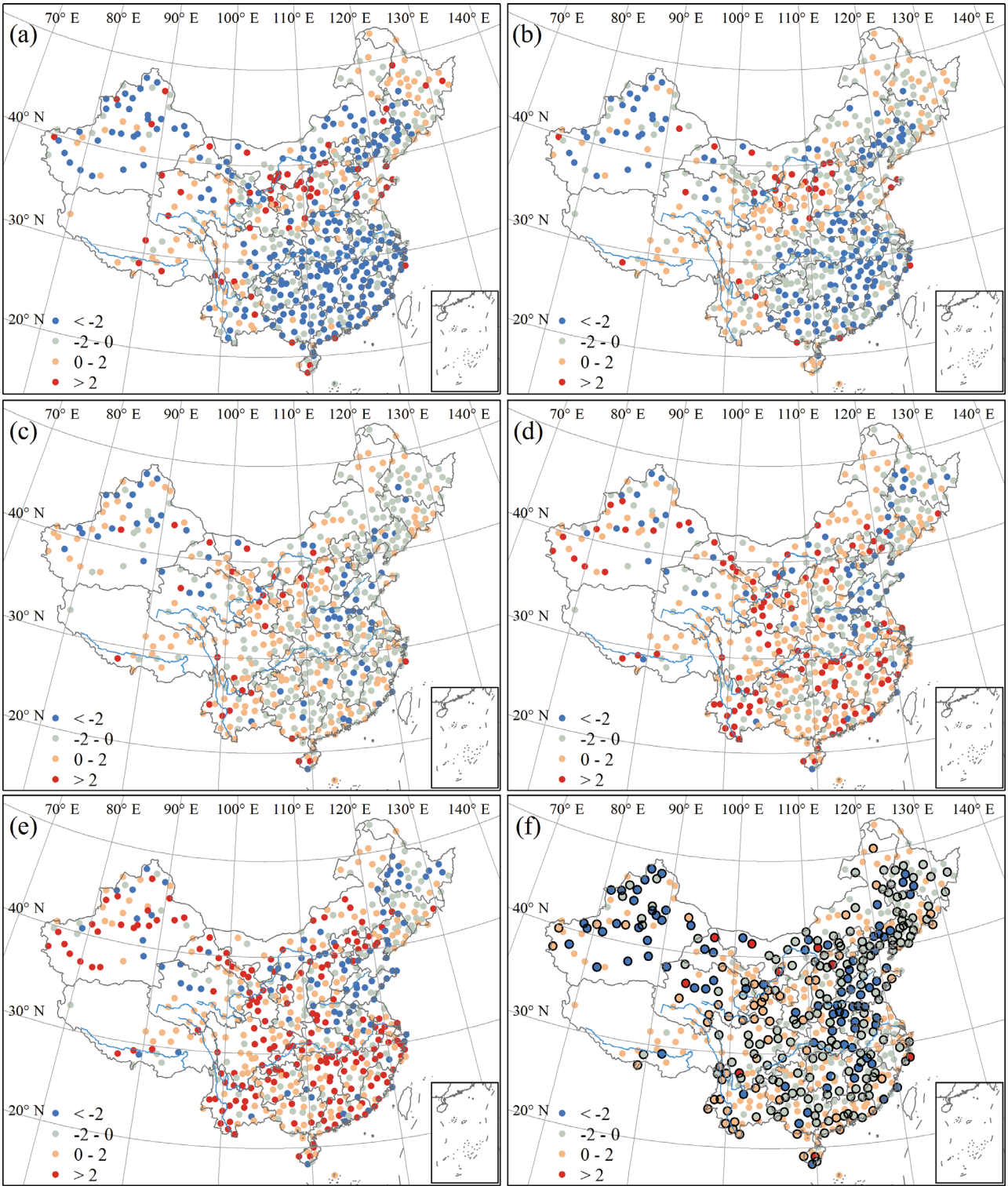

Fig. 3. Changing rate based on the EEMD trend in (a) 1970, (b) 1980, (c) 1990, (d) 2000 and (e) 2010 and based on the linear trend during (f) 1961–2015 for annual reference evapotranspiration (unit: mm yr^{-1}). Note that circles with an outline indicate statistical significance ($p < 0.05$)

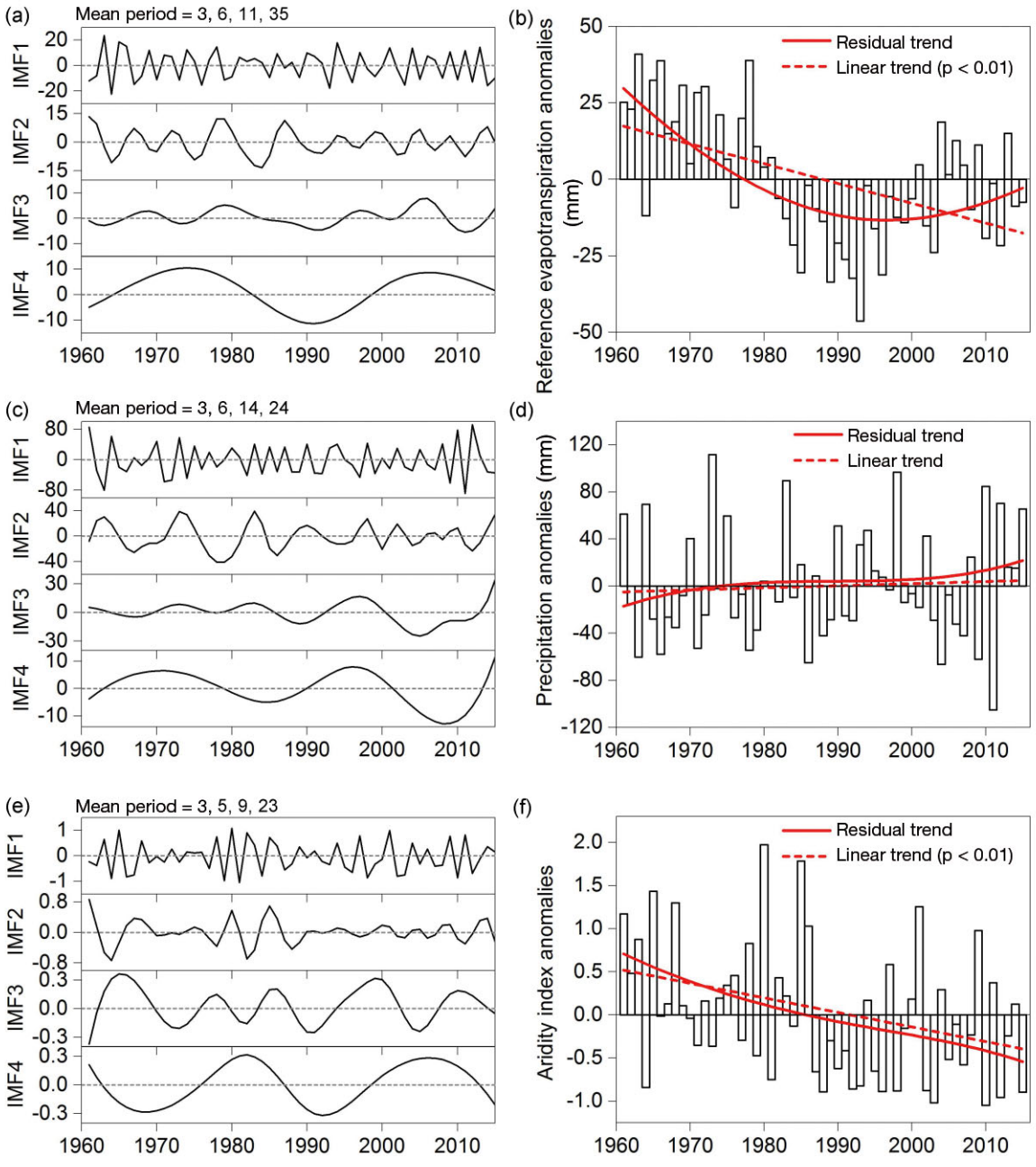

Fig. 4. EEMD components and linear trends of (a,b) annual reference evapotranspiration, (c,d) annual precipitation and (e,f) annual aridity index averaged over 573 stations during 1961–2015

residual trend in annual P had a decelerating upward trend before 1992, and then accelerated with an increasing trend during 1992–2015. The variance contribution rates of trend components in annual ET_o and P accounted for 40.00% and 2.77% of their total variability, respectively, illustrating that the nonlinear trend in annual ET_o had a relatively large influence on the characteristics of the original series, while the overall trend in annual P contained much less of the variability.

3.3. Changes in AI

After decomposing the annual AI during 1961–2015 using EEMD, the mean periods of IMF1, IMF2, IMF3 and IMF4 had similar patterns to that of P (Fig. 7). Most stations had an insignificant quasi 3 yr oscillation indicated by the IMF1 components. The IMF2 components showed mainly 5 and 6 yr quasi-periodic oscillations, with only 4.71% of the stations having statistically significant periods. The IMF3

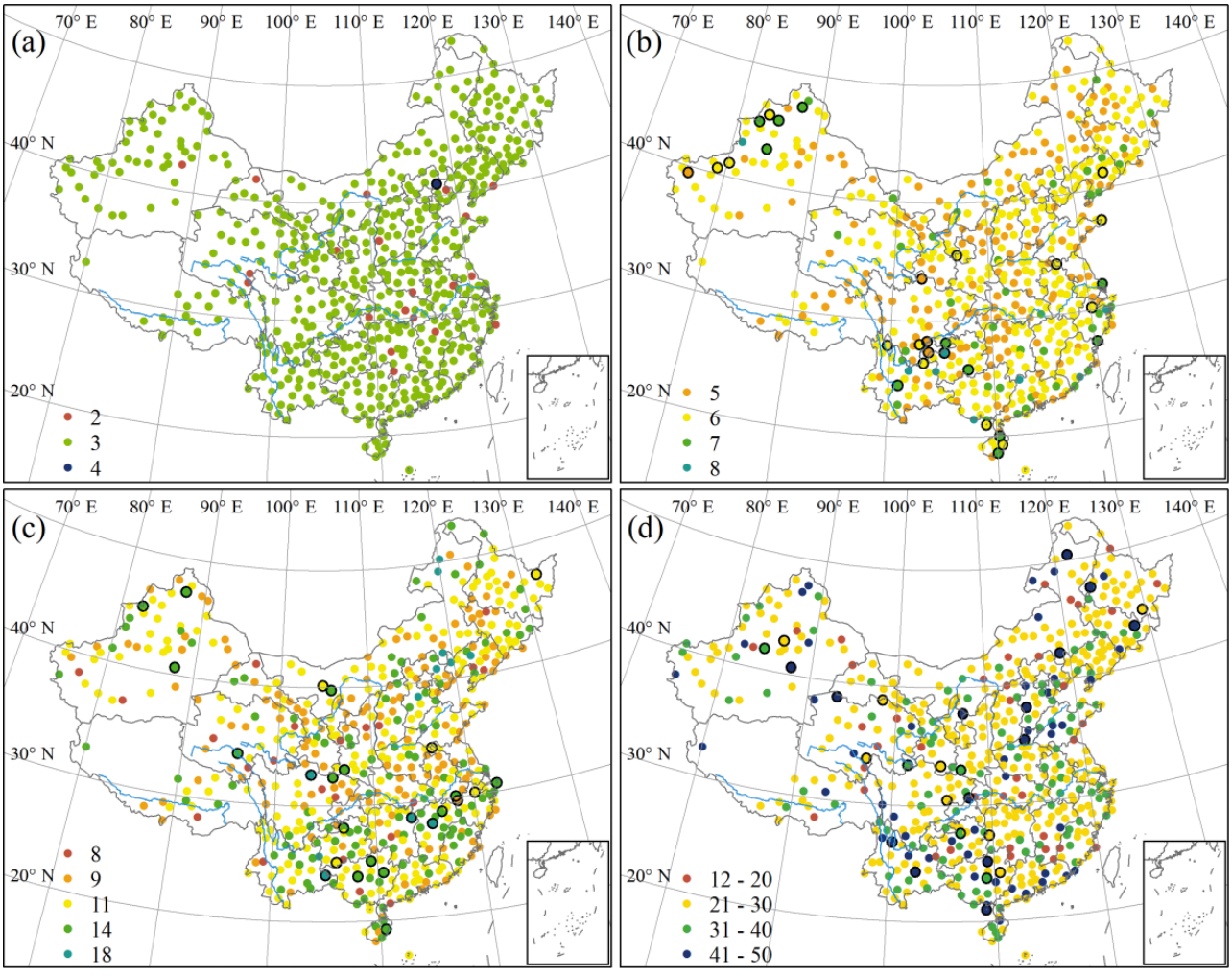

Fig. 5. Mean period of the EEMD components (a) IMF1, (b) IMF2, (c) IMF3 and (d) IMF4 for annual precipitation (unit: year). Note that circles with an outline indicate statistical significance ($p < 0.05$)

components indicated 11 and 14 yr oscillations, with only 5.58% of the stations being statistically significant. For IMF4, a few stations (8.55%) with statistically significant oscillations were scattered with a mean period of >20 yr.

Fig. 8 illustrates the spatial distributions of changes in annual AI during 1961–2015. According to the nonlinear variations in the EEMD trend (Figs. 8a–e), approximately 76.09% of the stations had reversed changes during 1961–2015. The annual AI decreased in 1970 in Northwest China, Inner Mongolia and the region south of the Huai River, whereas it increased in the Loess Plateau, North China Plain and east of Northeast China, mostly exceeding 0.005. In 1980, the changing rates of the annual AI slowed down in eastern Northeast China where it increased, and south of the Huai River where it decreased, mostly not exceeding 0.005. However, the annual AI reversed to increase in eastern Inner Mongolia in 1980. In 1990, the spatial pattern of the AI changes generally remained the same as in 1980 except that the annual AI reversed to decline in eastern Northeast China and south of the North China Plain. The changing rates of AI in 2000 were further enhanced in the same direction as in 1990. However, some of the stations reversed to decrease in the middle of the Loess Plateau and reversed to increase south of the Yangtze River in 2000. By 2010, the areas with stronger positive rates of AI >0.005 extended to 23.91% from 14.66% in 2000, and included most stations south of the Yangtze River and several stations in Northwest China. However, annual AI decreased in the middle of the Loess Plateau in 2010.

In general, the spatial pattern of linear trends during the past 55 yr was quite similar to the changing rates of the annual AI in 1990. A small number of sta-

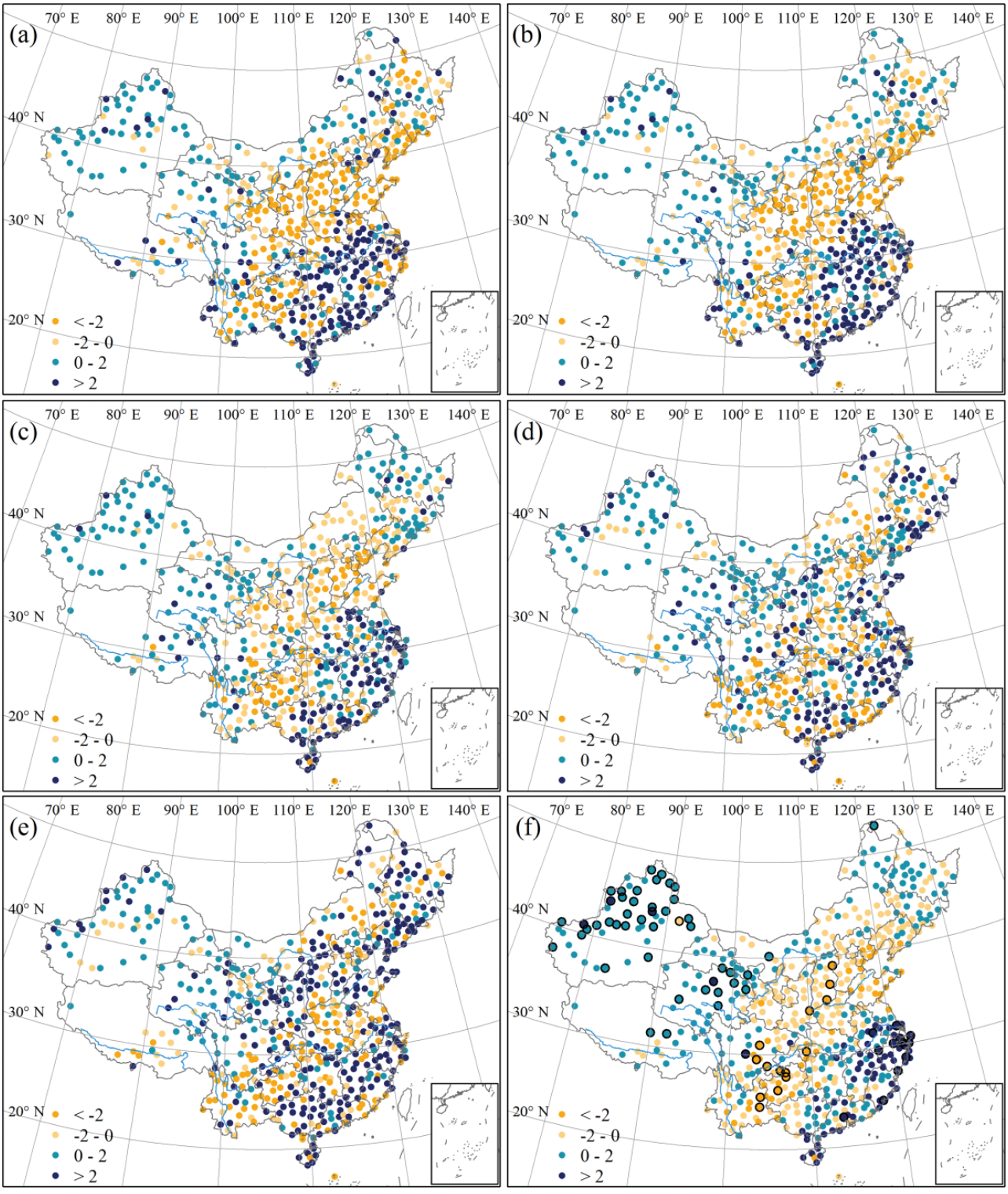

Fig. 6. Changing rate based on the EEMD trend in (a) 1970, (b) 1980, (c) 1990, (d) 2000 and (e) 2010 and based on the linear trend during (f) 1961–2015 for annual precipitation (unit: mm yr^{-1}). Note that circles with an outline indicate statistical significance ($p < 0.05$)

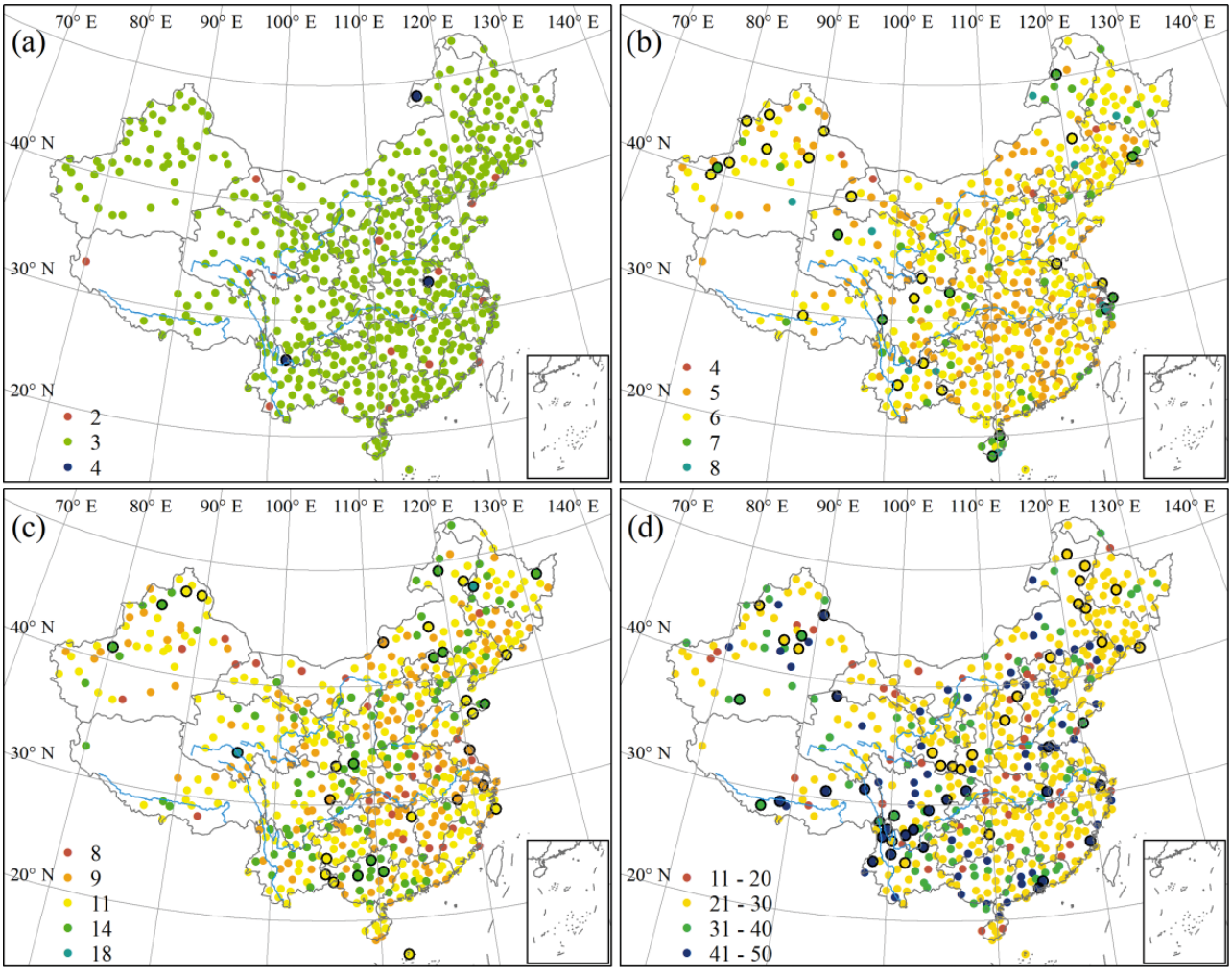

Fig. 7. Mean period of the EEMD components (a) IMF1, (b) IMF2, (c) IMF3 and (d) IMF4 for annual aridity index (unit: year). Note that circles with an outline indicate statistical significance ($p < 0.05$)

tions had upward trends in annual AI, which were mainly located in northern and western Northeast China, North China, north of the Loess Plateau and eastern Southwest China. Increasing trends above 0.005 yr^{-1} were concentrated mainly in the northern areas. At the same time, >64 % of the stations had linear downward trends in the annual AI, which were mainly distributed in Northwest China, the Tibetan Plateau, southern Northeast China, and the region south of the Huai River. Particularly, the annual AI had statistically significant decreasing trends in the northwest arid region, where monotonic decreases in the EEMD changing rates also occurred.

The average station values from the mean periods of IMF1, IMF2, IMF3 and IMF4 in AI were quasi 3 yr, quasi 5 yr, quasi 9 yr and quasi 23 yr (Fig. 4e). The hydroclimatic variables of ET_o, P and AI had similar interannual and decadal-scale quasi-periodic oscillations indicated by the first 3 IMFs. IMF1 contributed the greatest variance to the original time series, explaining approximately 34.06, 73.60 and 55.49 % of the total variability for annual ET_o, P and AI, respectively. It indicated that the AI oscillation on interannual to decadal time scales was mainly influenced by both ET_o and P. On timescales longer than 20 yr, the AI oscillation was mainly attributed to changes in P.

Averaged from all stations in China, the AI anomalies appeared to be mainly positive before 1986, and after 1986, they were usually negative (Fig. 4f). The linear trend exhibited a statistically significant decreasing trend of -0.02 ± 0.12 yr^{-1} SD ($p < 0.01$). At the same time, the EEMD residue of the annual AI declined continuously but with a decelerating to accel-

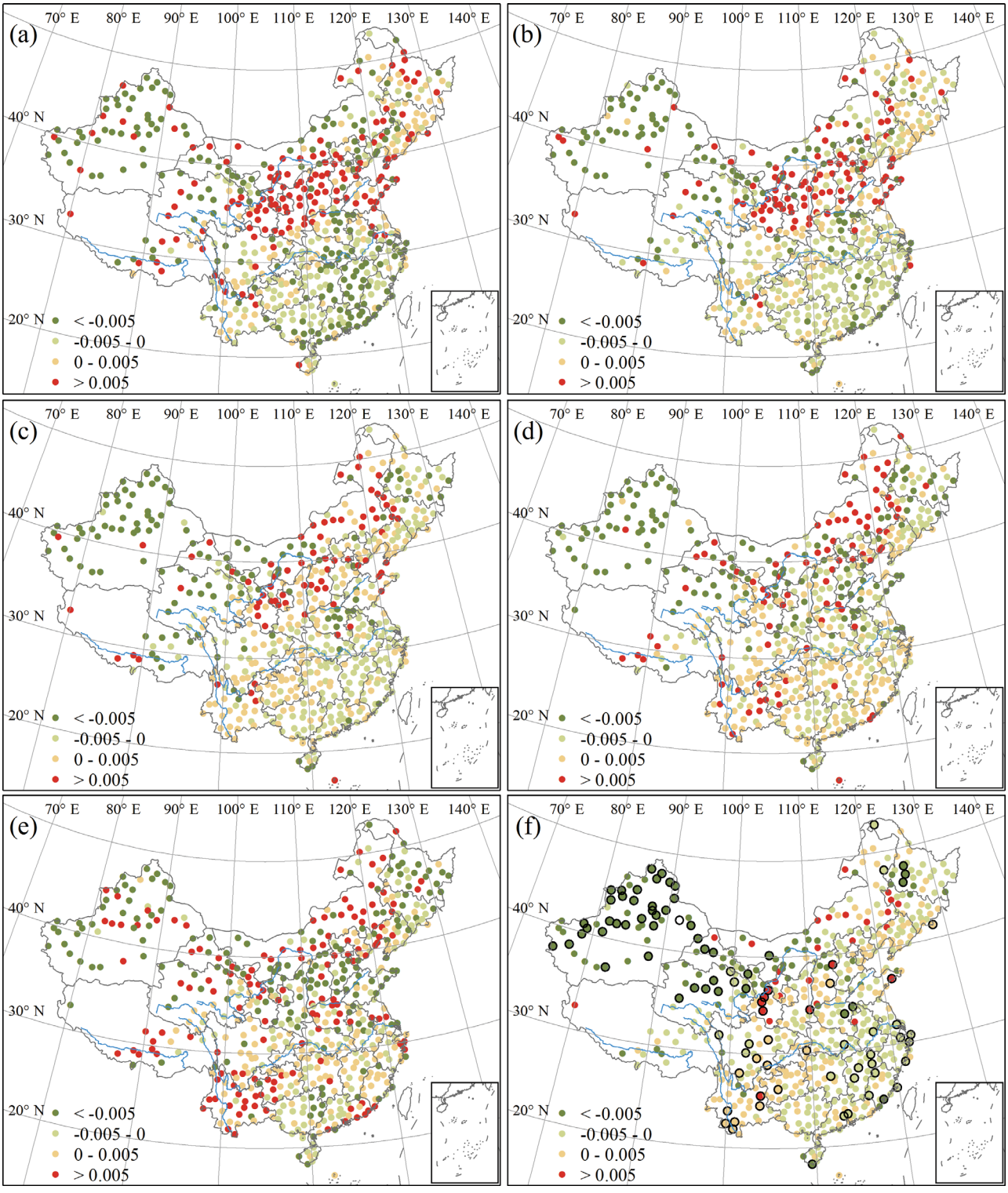

Fig. 8. Changing rate based on the EEMD trend in (a) 1970, (b) 1980, (c) 1990, (d) 2000 and (e) 2010 and based on the linear trend during (f) 1961–2015 for the annual aridity index (unit: yr^{-1}). Note that circles with an outline indicate statistical significance ($p < 0.05$)

erating rate, and the lowest rate occurred in 1997. The variance contribution rate of the residual trend in annual AI was 18.30% of its total variability. Comparing the overall linear trends of the hydroclimatic variables, the nonlinear variations were better suited to further reveal the time-varying trends and interdecadal transition of hydroclimatic variables in China.

3.4. Contribution of changes in annual P and ET_o to AI

We have illustrated the spatial-temporal variations in the AI that resulted from the synthesized changes in P and ET_o. To quantify the separate contribution of nonlinear change in a variable in different eco-geographical regions in China, we analyzed the changes in the AI between the original and recalculated series with the EEMD trend removed (Fig. 9).

Based on eco-geographical regionalization, the results illustrated that in most regions, the EEMD trend of ET_o or P produced a decrease in the AI over the past 55 yr. The P trend contributed more than the ET_o trend to the change in the AI in most regions. Compared to the original series, the decline in the AI caused by the ET_o trend averaged −1.38 ~ −7.86%, with the greatest change occurring in the mid-subtropical humid region; the trend of P reduced the AI by −3.28 ~ −15.23%, on average, and the most obvious reduction occurred in the tropical humid region and the northwest arid region. Particularly in the subtropical and northwest arid regions, the EEMD trend of both ET_o and P led to a decrease in the AI over the past 55 yr. In the northwest arid region, the trends of decreased ET_o and increased P during 1961–2015 led to an average declining ratio of −4.24% and −10.66% for the AI, respectively.

Moreover, there were also some regions where the AI was increased by the ET_o and/or P trends. For example, in the northern semi-arid region, the trends of increased ET_o and decreased P during 1961–2015 raised the AI by an average ratio of 1.34% and 9.66%, respectively. These may have negative implications for the current water scarcity in the semi-arid region. For temperate regions, tropical regions and the Tibetan Plateau region, the trends of ET_o and P had differing effects on the AI, among which the P trend played a leading role in the increase of the AI in warm temperate humid/sub-humid regions (15.51%) and in the decrease of the AI in the cold temperate humid region (−5.43%) and tropical humid region (−15.23%). The contributions of ET_o and P were comparable in degree but contrary in direction for the mid-temperate humid/sub-humid region (−2.68% and 3.20%) and the Tibetan Plateau region (2.46% and −5.04%).

Nonlinear changes of ET_o and P have complicated impacts on the regional AI in most regions. Because of the ET_o trend, the AI first decreased and then increased in the subtropical and tropical regions, where P changes contributed to the accelerated downward AI after 1997 in the north and mid-subtropical regions, with an average ratio of −4.00% and −5.00% during 1998–2015, respectively. In the mid-temperate and warm temperate humid/sub-humid regions as well as in the north semi-arid region, the AI first increased and then decreased, driven by nonlinear changes in P. These changes mostly appeared in the 1980s–1990s for the above regions. In the cold temperate region and northwest arid region, P induced the accelerating changes of AI after 1997, with an average ratio of −13.57% and −20.30%, respectively.

3.5. Correlations with changes in ENSO and PDO

We further explored the relationship of changes in aridity, as well as its determining factors, with large-scale climatic oscillations, including the ENSO and PDO. These relationships were measured by the Pearson correlation coefficients, and statistical significance was analyzed using a t-test. Fig. 10 illustrates the correlations of changes in the 3 variables with the SSTA over the Nino 3.4 region and the PDO index in different eco-geographical regions across China. Generally, in terms of the correlations in different eco-geographical regions, mid-temperate and warm temperate humid/sub-humid, north and south subtropical humid, north semi-arid and northwest arid regions were not appreciably affected, while the other regions suffered major impacts from the SSTA and PDO. The cold temperate humid and mid-subtropical humid regions were mainly affected by the PDO; the Tibetan Plateau region was mainly affected by the SSTA. Both the PDO and SSTA exerted obvious influences on the tropical humid region. Considering the lag effect of the ENSO event and the PDO phenomenon, the correlation analysis was further conducted for 1 yr lagged hydroclimatic variables with large-scale climatic oscillations. The result suggested that the SSTA also had effects on mid-temperate humid/sub-humid, north semi-arid and northwest arid regions.

Specifically, for the significant correlations, ET_o was negatively correlated with the PDO in both cold

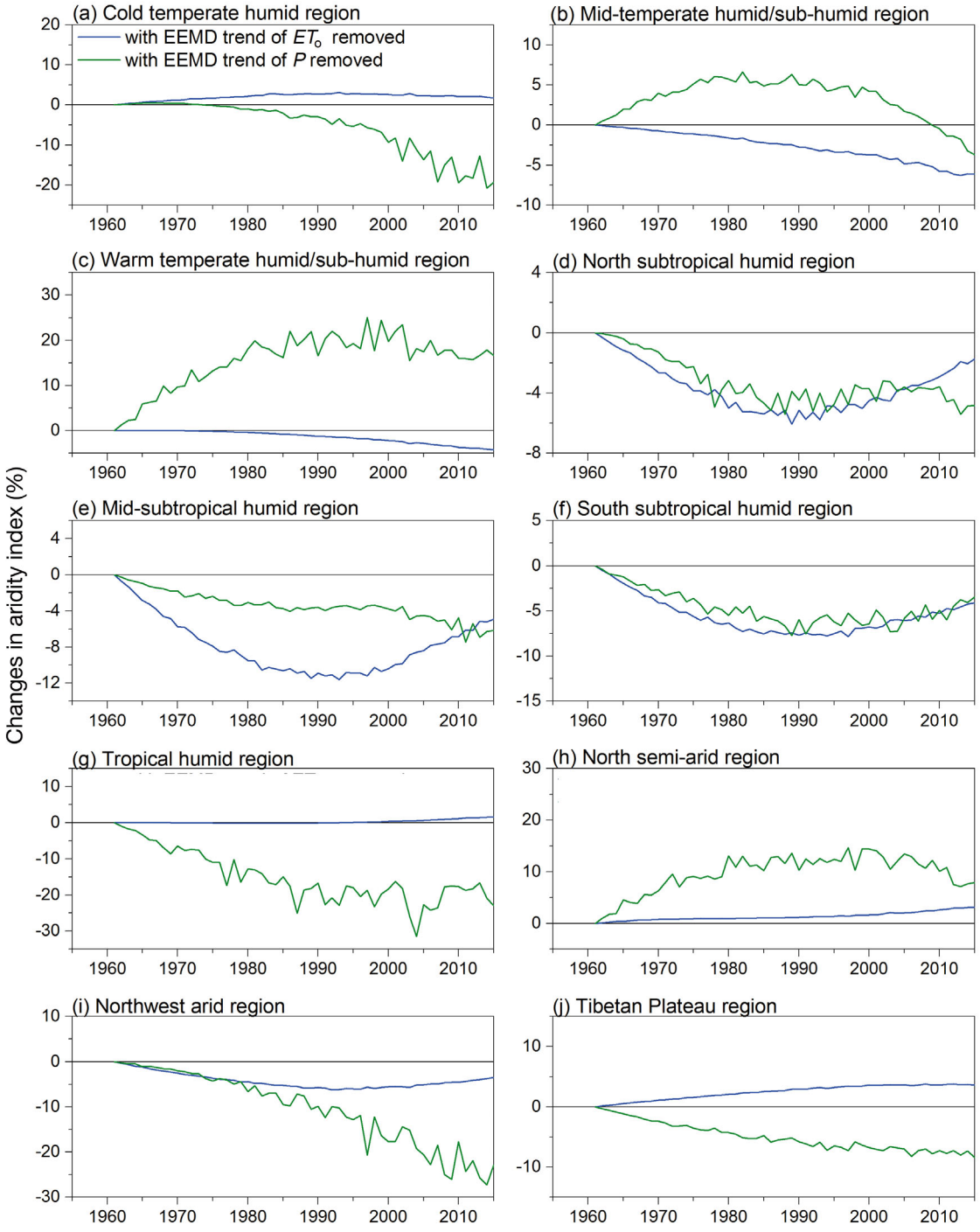

Fig. 9. Changes (%) in the aridity index (AI) between the original and recalculated series with the EEMD trend removed in different eco-geographical regions. A negative value indicates that a change in reference evapotranspiration (ET_o) or precipitation (P) causes a decrease in the AI, and a positive value indicates that an ET_o or P change causes an increase in the AI. Note differences in y-axis scales

temperate and mid-subtropical humid regions. For the mid-temperate humid/sub-humid region, the SSTA was positively correlated with the lagged P. P was negatively associated with the SSTA in the Tibetan Plateau region. Both SSTA and PDO were negatively related to P in the tropical humid region where ET_o was positively correlated with the SSTA and the lagged P was also negatively correlated with

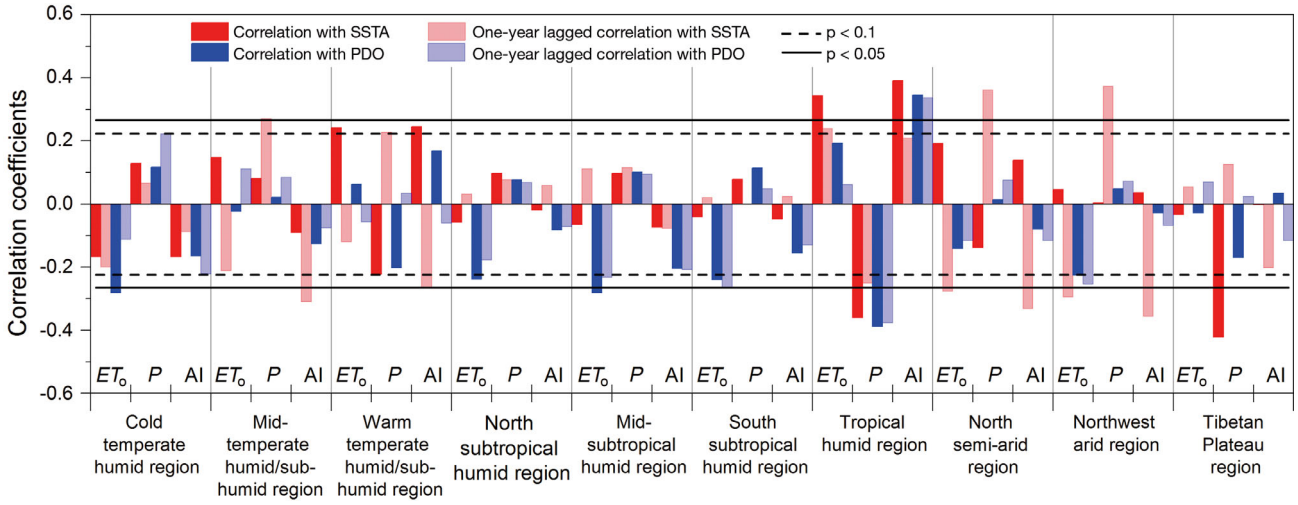

Fig. 10. Correlations of reference evapotranspiration (ET_o), precipitation (P) and the aridity index (AI) with the sea surface temperature anomaly (SSTA) over the Nino 3.4 region and the Pacific Decadal Oscillation (PDO) index in different eco-geographical regions

the PDO. For both north semi-arid and northwest arid regions, the lagged ET_o was negatively associated with the SSTA, yet the lagged P was positively associated with the SSTA.

Since large-scale climatic oscillations influenced the AI by affecting ET_o and P, the significant relationships of regional AI with the SSTA and PDO were reflected as follows. The lagged AI was negatively correlated with the SSTA in the mid-temperate humid/sub-humid, north semi-arid and northwest arid regions. Both the SSTA and PDO were positively correlated with the AI in the tropical humid regions where the lagged AI was also positively correlated with the PDO. For the cold temperate and mid-subtropical humid regions, as well as the Tibetan Plateau, there were obvious correlations between ET_o or P and large-scale climatic oscillations, but the correlations between the SSTA or PDO and the AI failed the significance test.

4. DISCUSSION

4.1. Nonlinear changes in aridity during 1961–2015

The linear trends of AI indicated in this study are in line with the results of Huang et al. (2017) and Chen et al. (2017), who identified a wetting trend distributed in regions west of 100° E, mainly including arid regions and the Tibetan Plateau, and a drying trend in a large part of regions east of 100° E, including semiarid and cold and temperate semi-humid regions in the past half century. Moreover, the climate system has evolved in a nonlinear and chaotic way. The EEMD is part of non-stationary methods such as networks, tipping point predictions and regime states, which lead to new physical insights into the climate system (Franzke 2014). Our study quantified the nonlinear changes of aridity in China during 1961–2015 based on the EEMD. Our results indicated that a continuous wetting trend occurred in Northwest China, which generally agreed with the findings of other studies (Huo et al. 2013, Liu et al. 2013, Wang et al. 2015). Consistent with our study, drying trends in Southwest China and east of Inner Mongolia were also reported in previous studies, e.g. Sun et al. (2016) and H. Zhang et al. (2016). Unlike previous studies, we further found that AI had nonlinear changes from decreasing to increasing mainly in Inner Mongolia and in the areas south of the middle and lower reaches of the Yangtze River, and changes from increasing to decreasing in the southern part of Northeast China, the east of the Loess Plateau and the southern North China Plain.

Compared with nonlinear changes in precipitation and aridity, there was a clear reversal for the nationally averaged ET_o, which was detected to be between 1997 and 1998 in China as a whole, and the reversal trends in the ET_o were also detected at 75.91% of the stations in China. The reversal from decreasing to increasing ET_o estimated in this study is consistent with research by Liu et al. (2011), who reported a decrease in annual pan evaporation during 1960–1991 and increases since 1992 through subsection linear fitting. A recent study also revealed a gener-

ally decreasing ET_o trend during 1956–2015 and an abrupt increase in the 1980s in most areas of China, except for the Tibetan Plateau in the 1990s (Fan et al. 2016). Similarly, although ET_o decreased significantly from 1981–1997, it has significantly increased since 1998 on the Tibetan Plateau (Yin et al. 2013). Nevertheless, the recent trend reversal suggested by these studies did not alter the overall downward trend of ET_o during the last several decades.

4.2. Attribution of the hydroclimatic changes

There are complicated mechanisms to explain the changes in the hydroclimatic variables. Our study indicated that the impacts from ET_o and P on the AI have large spatiotemporal variability due to their nonlinearity. In particular, their relative contributions differed greatly among the climate regions. The EEMD trend in P contributed more than the ET_o trend to the change in the AI in most eco-geographical regions in China during the past 55 yr, mainly including the temperate regions and western regions. Our results confirmed previous studies documenting contributions to regional aridity changes. For instance, it was estimated that the increase in precipitation has contributed more than the decrease in ET_o to the decreased AI in Northwest China over the last 5 decades (Huo et al. 2013). Increasing precipitation was indicated to be the dominant factor of the wetter climate in the Tibetan Plateau region by Gao et al. (2015). It should be mentioned that the limited ground-based precipitation information owing to a harsh environment on the Tibetan Plateau would produce more uncertainties in the regional results (Liu et al. 2017). Even though the AI did not explicitly show a reversal for China as a whole, the changing rate of the AI became positive since the 1990s in the subtropical regions due to the reversal in ET_o and P in the 1990s, indicating a potential shift from wet to dry. Relationships among P, ET_o and AI research for longer periods and on seasonal scales are needed to verify these results.

Aerodynamic and radiative components primarily determined the dynamics of annual atmospheric evaporative demand (McVicar et al. 2012b). The dominant factor varied for different regions. During the last several decades, the widely decreased annual atmospheric evaporative demand has been mainly attributed to declining near-surface wind speed in the Tibetan Plateau (Chen et al. 2006, Y. Zhang et al. 2007, X. Zhang et al. 2009), North China (Xu et al. 2006, Yin et al. 2010) and some other mid-latitude regions worldwide (McVicar et al. 2012a). Moreover, solar radiation is the dominant source of energy at the land surface. Our previous study suggested that the reduced sunshine duration was the decisive factor to explain the decreasing trend in ET_o in south China in the past decades (Yin et al. 2010). At a global scale, solar radiation has changed from dimming to brightening, with a reversal occurring around ca. 1990 since the 1950s, which was possibly due to the interaction between direct and indirect effects of aerosols (Wild et al. 2005). The reversed trend is consistent with the changes in annual ET_o for south China in this study. Rising temperature was suggested to be largely responsible for the recent upward trend in pan evaporation observations in China (Liu et al. 2011). Also, the recent increase in ET_o values was affected by the aggregated emission of greenhouse gases and air pollution from energy consumption (Fan et al. 2016).

Large-scale climatic oscillations, including ENSO and PDO, have had substantial links to the changes in the hydroclimatic variables in some regions in China. Specifically, the 1 yr lagged responses of ET_o and P to the SSTA were more pronounced than the contemporary correlations in the medium temperate zone extending from 35 to 50° N. Precipitation in northwestern China was probably also related to westerly circulation and topographical factors (Shi et al. 2016), and other climate indices, such as the Arctic Oscillation and North Atlantic Oscillation, were reported to play an important role in the drought evolution as well (Wang et al. 2015). Zhang et al. (2017) found that the impact of ENSO on AI overweighed the Arctic Oscillation effects on AI in northern China during the past 5 decades, particularly on the timescale of 2–6 yr. Moreover, the multidecadal variability of aridity in north China was significantly correlated with the PDO phase changes during the last century (Qian & Zhou 2014). Furthermore, multiscale characteristics of the relationship between large-scale ocean–atmosphere interactions and aridity need to be examined in future studies. Exploring these relationships would help to improve the ability to forecast regional drought (Wang et al. 2014, Z. Liu et al. 2016, Xiao et al. 2016, Zhang et al. 2017).

This study provided a deep and promising perspective for detecting and attributing the hydrological response to climate change, which would have profound implications for understanding hydrological processes and estimating water use efficiency and the response of both of these factors to climate change, as well as agricultural irrigation and optimal allocation of water resources. Besides aridity change,

human activities also have significant impacts on hydrological processes, such as actual evapotranspiration and runoff (Liu et al. 2012, Douville et al. 2013, B. Zhang et al. 2016). Changes in vegetation type, due to deforestation for example, can play an important role in partitioning the catchment water yield (Woodward et al. 2014, Q. Liu et al. 2016). Indeed, in regions with intensive human activities like China's Loess Plateau where the Grain-for-Green project was implemented, ecological restoration and more efficient water management practices could have much larger contributions to streamflow changes than those of climate change (Liu & McVicar 2012, Liang et al. 2015). The above implies the importance of quantifying the interactive role that hydroclimatic changes and anthropogenic influences play in regional hydrological processes and water resources management.

5. CONCLUSION

Based on 573 stations and a nonlinear and nonstationary processing method using EEMD, we investigated the nonlinear variability and spatial differences in aridity and their influencing climatic variables in China from 1961–2015. Furthermore, the contributions of ET_o and P on the AI and their links to variations in the ENSO and PDO were also explored. The primary conclusions are as follows:

(1) Aridity had evident nonlinear variations with spatial differences. Particularly, 57.42% of the stations had decreased AI during 1961–2015. About half of these stations showed reversals from decreasing to increasing AI, primarily distributed in areas south of the middle and lower reaches of the Yangtze River. In contrast, increased AI with reversals, from increasing to decreasing (20.94%), largely focused on the east of the Loess Plateau, which indicated a wetter trend emerging since the late 1990s, although a relatively arid status was still dominant.

(2) The majority of the stations experienced reversals from downward to upward trends of ET_o (53.92%), and mostly occurred around the 1990s in South China and Northwest China, where the enhancement effects of such reversed ET_o trends on AI were offset by the increment of P. If the offset degree was large enough, it could induce a continuously downward AI, as observed at the majority of stations in Northwest China.

(3) At the regional scale, the nonlinear changes in AI were determined by combined effects of ET_o and P. Comparatively, the contribution of the P trend to the regional AI was larger than the ET_o trend, except in the subtropical regions, where ET_o variations also played a key role. The significant spatial difference and distinct multiscale variations of aridity both suggest that ET_o and P should be synthesized, and nonlinear changes could provide more specifics on hydroclimatic variations.

Acknowledgements. This work was supported by the National Natural Science Foundation of China (41571043), the Key Program of the National Natural Science Foundation of China (41530749), the Strategic Priority Research Program of the Chinese Academy of Sciences (XDA05090304) and the Cultivate Project of the Institute of Geographic Sciences and Natural Resources Research, Chinese Academy of Sciences (TSYJS03).

LITERATURE CITED

Allen RG, Pereira LS, Raes D, Smith M (1998) Crop evapotranspiration: guidelines for computing crop water requirements. FAO Irrigation and Drainage Paper 56. Food and Agriculture Organization of the United Nations, Rome

Arora VK (2002) The use of the aridity index to assess climate change effect on annual runoff. J Hydrol (Amst) 265:164–177

Basha G, Ouarda TBMJ, Marpu PR (2015) Long-term projections of temperature, precipitation and soil moisture using non-stationary oscillation processes over the UAE region. Int J Climatol 35:4606–4618

Carmona AM, Poveda G (2014) Detection of long-term trends in monthly hydro-climatic series of Colombia through empirical mode decomposition. Clim Change 123:301–313

Chang NB, Vasquez MV, Chen CF, Imen S, Mullon L (2015) Global nonlinear and nonstationary climate change effects on regional precipitation and forest phenology in Panama, Central America. Hydrol Processes 29:339–355

Chen SB, Liu YF, Thomas A (2006) Climatic change on the Tibetan Plateau: potential evapotranspiration trends from 1961–2000. Clim Change 76:291–319

Chen T, Zhang H, Chen X, Hagan DF, Wang G, Gao Z, Shi T (2017) Robust drying and wetting trends found in regions over China based on Köppen climate classifications. J Geophys Res Atmos 122:4228–4237

Cook BI, Smerdon JE, Seager R, Coats S (2014) Global warming and 21st century drying. Clim Dyn 43:2607–2627

Dai AG (2013) Increasing drought under global warming in observations and models. Nat Clim Chang 3:52–58

Delgado-Baquerizo M, Maestre FT, Gallardo A, Bowker MA and others (2013) Decoupling of soil nutrient cycles as a function of aridity in global drylands. Nature 502:672–676

Dolman AJ, de Jeu RAM (2010) Evaporation in focus. Nat Geosci 3:296

Douville H, Ribes A, Decharme B, Alkama R, Sheffield J (2013) Anthropogenic influence on multidecadal changes in reconstructed global evapotranspiration. Nat Clim Chang 3:59–62

Fan JL, Wu LF, Zhang FC, Xiang YZ, Zheng J (2016) Climate change effects on reference crop evapotranspiration across different climatic zones of China during 1956–2015. J Hydrol (Amst) 542:923–937

Feng S, Fu Q (2013) Expansion of global drylands under a warming climate. Atmos Chem Phys 13:10081–10094
Franzke C (2012) Nonlinear trends, long-range dependence, and climate noise properties of surface temperature. J Clim 25:4172–4183
Franzke CLE (2014) Warming trends: nonlinear climate change. Nat Clim Chang 4:423–424
Gao Y, Li X, Leung LR, Chen D, Xu J (2015) Aridity changes in the Tibetan Plateau in a warming climate. Environ Res Lett 10:034013
Good P, Lowe JA, Andrews T, Wiltshire A and others (2015) Nonlinear regional warming with increasing CO_2 concentrations. Nat Clim Chang 5:138–142
Greve P, Seneviratne SI (2015) Assessment of future changes in water availability and aridity. Geophys Res Lett 42:5493–5499
Greve P, Orlowsky B, Mueller B, Sheffield J, Reichstein M, Seneviratne SI (2014) Global assessment of trends in wetting and drying over land. Nat Geosci 7:716–721
Guo B, Chen Z, Guo J, Liu F, Chen C, Liu K (2016) Analysis of the nonlinear trends and non-stationary oscillations of regional precipitation in Xinjiang, northwestern China, using ensemble empirical mode decomposition. Int J Environ Res Public Health 13:345
Hobbins MT, Ramirez JA, Brown TC (2004) Trends in pan evaporation and actual evapotranspiration across the conterminous U.S.: paradoxical or complementary? Geophys Res Lett 31:L13503
Huang JP, Yu HP, Guan XD, Wang GY, Guo RX (2016) Accelerated dryland expansion under climate change. Nat Clim Chang 6:166–171
Huang NE, Wu Z (2008) A review on Hilbert-Huang transform: method and its applications to geophysical studies. Rev Geophys 46:RG2006
Huang NE, Shen Z, Long SR, Wu MC and others (1998) The empirical mode decomposition method and the Hilbert spectrum for non-stationary time series analysis. Proc R Soc A 454:903–995
Huang Q, Zhang Q, Singh VP, Shi P, Zheng Y (2017) Variations of dryness/wetness across China: changing properties, drought risks, and causes. Global Planet Change 155:1–12
Huo Z, Dai X, Feng S, Kang S, Huang G (2013) Effect of climate change on reference evapotranspiration and aridity index in arid region of China. J Hydrol (Amst) 492:24–34
Ji F, Wu Z, Huang J, Chassignet EP (2014) Evolution of land surface air temperature trend. Nat Clim Chang 4:462–466
Kukal M, Irmak S (2016) Long-term patterns of air temperatures, daily temperature range, precipitation, grass-reference evapotranspiration and aridity index in the USA Great Plains. I. Spatial trends. J Hydrol (Amst) 542: 953–977
Kuo CC, Gan TY, Chan S (2013) Regional intensity-duration-frequency curves derived from ensemble empirical mode decomposition and scaling property. J Hydrol Eng 18: 66–74
Li B, Chen Z, Yuan X (2015) The nonlinear variation of drought and its relation to atmospheric circulation in Shandong Province, East China. PeerJ 3:e1289,
Li Y, Yao N, Chau HW (2017) Influences of removing linear and nonlinear trends from climatic variables on temporal variations of annual reference crop evapotranspiration in Xinjiang, China. Sci Total Environ 592:680–692
Liang W, Bai D, Wang F, Fu B and others (2015) Quantifying the impacts of climate change and ecological restoration on streamflow changes based on a Budyko hydrological model in China's Loess Plateau. Water Resour Res 51: 6500–6519
Liu M, Tian H, Lu C, Xu X, Chen G, Ren W (2012) Effects of multiple environment stresses on evapotranspiration and runoff over eastern China. J Hydrol (Amst) 426–427: 39–54
Liu Q, McVicar TR (2012) Assessing climate change induced modification of Penman potential evaporation and runoff sensitivity in a large water-limited basin. J Hydrol (Amst) 464–465:352–362
Liu Q, McVicar TR, Yang Z, Donohue RJ, Liang L, Yang Y (2016) The hydrological effects of varying vegetation characteristics in a temperate water-limited basin: development of the dynamic Budyko-Choudhury-Porporato (dBCP) model. J Hydrol 543B:595–611
Liu XM, Luo YZ, Zhang D, Zhang MH, Liu CM (2011) Recent changes in pan-evaporation dynamics in China. Geophys Res Lett 38:L13404
Liu X, Zhang D, Luo Y, Liu C (2013) Spatial and temporal changes in aridity index in northwest China: 1960 to 2010. Theor Appl Climatol 112:307–316
Liu X, Yang T, Hsu K, Liu C, Sorooshian S (2017) Evaluating the streamflow simulation capability of PERSIANN-CDR daily rainfall products in two river basins on the Tibetan Plateau. Hydrol Earth Syst Sci 21:169–181
Liu Z, Menzel L, Dong C, Fang R (2016) Temporal dynamics and spatial patterns of drought and the relation to ENSO: a case study in Northwest China. Int J Climatol 36: 2886–2898
McCabe GJ, Wolock DM (2002) Trends and temperature sensitivity of moisture conditions in the conterminous United States. Clim Res 20:19–29
McVicar TR, Roderick ML, Donohue RJ, Li LT and others (2012a) Global review and synthesis of trends in observed terrestrial near-surface wind speeds: implications for evaporation. J Hydrol (Amst) 416-417:182–205
McVicar TR, Roderick ML, Donohue RJ, Niel TGV (2012b) Less bluster ahead? Ecohydrological implications of global trends of terrestrial near-surface wind speeds. Ecohydrology 5:381–388
Moral FJ, Paniagua LL, Rebollo FJ, García-Martín A (2017) Spatial analysis of the annual and seasonal aridity trends in Extremadura, southwestern Spain. Theor Appl Climatol 130:917–932
Mueller B, Zhang XB (2016) Causes of drying trends in northern hemispheric land areas in reconstructed soil moisture data. Clim Change 134:255–267
Partal T (2012) Wavelet analysis and multi-scale characteristics of the runoff and precipitation series of the Aegean region (Turkey). Int J Climatol 32:108–120
Peterson TC, Golubev VS, Groisman PY (1995) Evaporation losing its strength. Nature 377:687–688
Qian C, Zhou TJ (2014) Multidecadal variability of north China aridity and its relationship to PDO during 1900–2010. J Clim 27:1210–1222
Qian C, Fu C, Wu Z, Yan Z (2009) On the secular change of spring onset at Stockholm. Geophys Res Lett 36:267–272
Roderick ML, Farquhar GD (2002) The cause of decreased pan evaporation over the past 50 years. Science 298: 1410–1411
Roderick ML, Greve P, Farquhar GD (2015) On the assessment of aridity with changes in atmospheric CO_2. Water Resour Res 51:5450–5463
Schimel DS, Braswell BH, Parton WJ (1997) Equilibration of

the terrestrial water, nitrogen, and carbon cycles. Proc Natl Acad Sci USA 94:8280–8283
Sheffield J, Wood EF, Roderick ML (2012) Little change in global drought over the past 60 years. Nature 491:435–438
Sherwood S, Fu Q (2014) A drier future? Science 343:737–739
Shi P, Yang T, Zhang K, Tang Q, Yu Z, Zhou X (2016) Large-scale climate patterns and precipitation in an arid endorheic region: linkage and underlying mechanism. Environ Res Lett 11:044006
Sneyers R (1990) On the statistical analysis of series of observations. Tech Note 143. World Meteorological Society, Geneva
Sun C, Ma Y (2015) Effects of non-linear temperature and precipitation trends on Loess Plateau droughts. Quat Int 372:175–179
Sun S, Chen H, Wang G, Li J and others (2016) Shift in potential evapotranspiration and its implications for dryness/wetness over Southwest China. J Geophys Res Atmos 121:9342–9355
Tabari H, Aghajanloo MB (2013) Temporal pattern of aridity index in Iran with considering precipitation and evapotranspiration trends. Int J Climatol 33:396–409
Trenberth KE, Dai AG, van der Schrier G, Jones PD, Barichivich J, Briffa KR, Sheffield J (2014) Global warming and changes in drought. Nat Clim Chang 4:17–22
Wang H, Chen Y, Pan Y (2015) Characteristics of drought in the arid region of northwestern China. Clim Res 62: 99–113
Wang L, Cao L, Deng X, Jia P and others (2014) Changes in aridity index and reference evapotranspiration over the central and eastern Tibetan Plateau in China during 1960–2012. Quat Int 349:280–286
Wild M, Gilgen H, Roesch A, Ohmura A and others (2005) From dimming to brightening: decadal changes in solar radiation at Earth's surface. Science 308:847–850
Williams AP, Allen CD, Millar CI, Swetnam TW, Michaelsen J, Still CJ, Leavitt SW (2010) Forest responses to increasing aridity and warmth in the southwestern United States. Proc Natl Acad Sci USA 107:21289–21294
Woodward C, Shulmeister J, Larsen J, Jacobsen GE, Zawadzki A (2014) Landscape hydrology. The hydrological legacy of deforestation on global wetlands. Science 346:844–847
Wu SH, Yin YH, Zheng D, Yang QY (2006) Moisture conditions and climate trends in China during the period 1971–2000. Int J Climatol 26:193–206
Wu SH, Zheng D, Yin YH, Lin ED, Xu YL (2010) Northward-shift of temperature zones in China's eco-geographical study under future climate scenario. J Geogr Sci 20: 643–651
Wu Z, Huang NE (2004) A study of the characteristics of white noise using the empirical mode decomposition method. Proc R Soc A 460:1597–1611
Wu Z, Huang NE (2009) Ensemble empirical mode decomposition: a noise-assisted data analysis method. Adv Adapt Data Anal 01:1–41
Wu Z, Huang NE, Wallace J, Smoliak B, Chen X (2011) On the time-varying trend in global-mean surface temperature. Clim Dyn 37:759–773
Xiao M, Zhang Q, Singh VP, Liu L (2016) Transitional properties of droughts and related impacts of climate indices in the Pearl River basin, China. J Hydrol (Amst) 534:397–406
Xu M, Chang CP, Fu CB, Qi Y, Robock A, Robinson D, Zhang HM (2006) Steady decline of east Asian monsoon winds, 1969-2000: evidence from direct ground measurements of wind speed. J Geophys Res 111:D24111
Xue CF, Hou W, Zhao JH, Wang SG (2013) The application of ensemble empirical mode decomposition method in multiscale analysis of region precipitation and its response to the climate change. Wuli Xuebao 62:109203
Xue YK, Sun SF, Lau KM, Ji JJ and others (2005) Multiscale variability of the river runoff system in China and its long-term link to precipitation and sea surface temperature. J Hydrometeorol 6:550–570
Yin YH, Wu SH, Zheng D, Yang QY (2008) Radiation calibration of FAO56 Penman-Monteith model to estimate reference crop evapotranspiration in China. Agric Water Manag 95:77–84
Yin YH, Wu SH, Chen G, Dai EF (2010) Attribution analyses of potential evapotranspiration changes in China since the 1960s. Theor Appl Climatol 101:19–28
Yin YH, Wu SH, Zhao DS (2013) Past and future spatiotemporal changes in evapotranspiration and effective moisture on the Tibetan Plateau. J Geophys Res Atmos 118: 10850–10860
Yin Y, Ma D, Wu S, Pan T (2015) Projections of aridity and its regional variability over China in the mid-21st century. Int J Climatol 35:4387–4398
Yu HL, Lin YC (2015) Analysis of space–time non-stationary patterns of rainfall–groundwater interactions by integrating empirical orthogonal function and cross wavelet transform methods. J Hydrol (Amst) 525:585–597
Zarch MAA, Sivakumar B, Sharma A (2015) Assessment of global aridity change. J Hydrol (Amst) 520:300–313
Zhang B, He C, Burnham M, Zhang L (2016) Evaluating the coupling effects of climate aridity and vegetation restoration on soil erosion over the Loess Plateau in China. Sci Total Environ 539:436–449
Zhang H, Zhang Q, Yue P, Zhang L, Liu Q, Qiao S, Yan P (2016) Aridity over a semi-arid zone in Northern China and responses to the East Asian Summer Monsoon. J Geophys Res Atmos 121:13901–13918
Zhang K, Qian X, Liu P, Xu Y, Cao L, Hao Y, Dai S (2017) Variation characteristics and influences of climate factors on aridity index and its association with AO and ENSO in northern China from 1961 to 2012. Theor Appl Climatol 130:523–533
Zhang XQ, Ren Y, Yin ZY, Lin ZY, Du Z (2009) Spatial and temporal variation patterns of reference evapotranspiration across the Qinghai-Tibetan Plateau during 1971–2004. J Geophys Res 114:D15105
Zhang Y, Wallace JM, Battisti DS (1997) ENSO-like interdecadal variability: 1900-93. J Clim 10:1004–1020
Zhang YQ, Liu CM, Tang YH, Yang YH (2007) Trends in pan evaporation and reference and actual evapotranspiration across the Tibetan Plateau. J Geophys Res 112:D12110
Zhao Y, Zou X, Zhang J, Cao L, Xu X, Zhang K, Chen Y (2014) Spatio-temporal variation of reference evapotranspiration and aridity index in the Loess Plateau Region of China, during 1961–2012. Quat Int 349:196–206
Zheng D (2000) A study on the eco-geographic regional system of China. Proc FAO FRA2000 Global Ecological Zoning Workshop, 28–-30 Jul 1999, Cambridge, UK. FAO, Rome

Editorial responsibility: Eduardo Zorita, Geesthacht, Germany

Submitted: August 17, 2017; Accepted: November 3, 2017
Proofs received from author(s): February 18, 2018